ELSEVIER

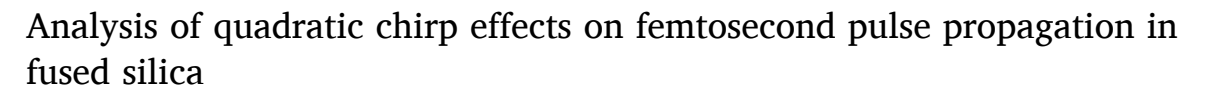
Contents lists available at ScienceDirect

Physics Letters A

journal homepage: www.elsevier.com/locate/pla



Discussion





Jing Hu, Lihe Yan*, Jinhai Si, Qinjun Jian, Xun Hou

Key Laboratory for Physical Electronics and Devices of the Ministry of Education & Shaanxi Key Lab of Photonic Technique for information, School of Electronics science & Engineering, Faculty of Electronic and Information Engineering, Xi'an Jiaotong University, Xi'an, 710049, PR China

ARTICLE INFO

Keywords Femtosecond pulse Nonlinear chirp Nonlinear Kerr effect

ABSTRACT

The effects of linear chirp (LC), quadratic chirp (QC), and the combined linear and quadratic chirps (L-QC) on the spatio-temporal and spectral properties of femtosecond pulses propagation taking into account the diffraction, group-velocity dispersion and self-focusing effects are studied. We conduct a detailed analysis of the distinct roles played by LC and QC components in L-QC pulse. The results indicate that, compared with LC pulse, the incorporation of QC in L-QC pulse aids in achieving further compression of both the pulse duration and beam width, while also enabling the adjustment of the latency time of peak intensity. On the other hand, compared with QC pulse, the inclusion of the LC component in the L-QC pulse facilitates easier adjustment of the spectral width, enabling it to be broadened or narrowed. The results demonstrate that the L-QC pulse exhibits greater adjustability, allowing for modulation of the intensity and spectral distributions of the pulse by adjusting respective contributions and parameters of the LC and QC.

1. Introduction

Femtosecond lasers have found widespread applications across various fields, including material processing [1,2], biomedicine [3,4], remote sensing [5,6], and optical solitons [7-19], among others. A thorough understanding of the propagation characteristics of femtosecond laser pulses is essential for optimizing their applications. For instance, femtosecond laser filamentation in air has been utilized for pollutant detection [20,21] and lightning control [22,23], wherein controlling the spatial and spectral distributions of the laser is crucial for its long-distance propagation. Moreover, in the realm of laser micro-nano processing, the spatial and temporal characteristics of the focused femtosecond laser significantly influence machining accuracy and efficiency [24]. Generally, the propagation of intense femtosecond laser pulses in media is governed by both linear and nonlinear optical effects, including diffraction, group velocity dispersion (GVD), self-focusing (SF), and self-phase modulation (SPM) effects. These effects can affect modify the pulse's spectral distribution by introducing new frequency components and may lead to pulse splitting [25,26].

The propagation of chirped pulses has been a subject of significant theoretical and practical interest for an extended period. The chirp plays an important role in optical pulse compressors [27], optical soliton

communications [28], extension of the supercontinuum [29,30], and extension of filamentation length [31,32], while chirp with different forms, i.e., linear chirp and kinds of nonlinear chirps, could affect the propagation properties of femtosecond pulses. In previous reports, the influence of linear chirp on the pulse propagation has been widely studied [33,34]. It has been demonstrated that, pulses with a negative linear chirp have been shown to achieve a smaller beam spot, a compressed pulse width, and a narrower spectral width compared with those with positive chirp in normally dispersive media [35–41]. Additionally, the chirp can influence pulse focusing, where the number and location of foci can be controlled by changing the chirp value [42].

In addition to linear chirp, various forms of nonlinear chirp, including quadratic, Gaussian, exponential, and sinusoidal chirps [43] are inevitably introduced as the intense laser pulse propagates through nonlinear materials [25,44] and could also be generated by the acousto-optic dispersion delay line (AODDL) [45], thereby influencing pulse's propagation properties. Before, the diverse effects of time-dependent nonlinear chirps on the pulse propagation properties have been elucidated through the derivation of analytical linear propagation formulas [43]. On the other hand, in the event that the nonlinear effects of medium are taken into account, for example, in the presence of the cubic nonlinear Kerr effect, detailed studies have been conducted on

E-mail address: liheyan@mail.xjtu.edu.cn (L. Yan).

^{*} Corresponding author.

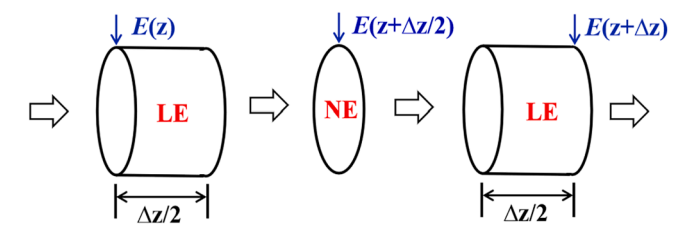


Fig. 1. The schematic diagram of the split-step method, LE: linear effects, NE: nonlinear effects.

the effects of higher order frequency-dependent nonlinear chirp on the intensity and spectral distributions of pulses [46]. Additionally, the influences of Kerr effect on the spectrum of nonlinear chirped pulse also have been reported [47]. Furthermore, there exists a novel class of self-similar solitary waves characterized by a nonlinear chirp which are generated by higher-order nonlinear effect [48–50]. However, in actual applications and experiments, the chirp is often not monotonically linear or nonlinear; rather, it is a complex chirp that contains both linear and nonlinear components under strong nonlinearity. Although a study has been conducted to explore the spectral distribution properties of complex chirped pulses containing quadratic and cubic [51], the combined effect along with a potential linear component was not discussed. Therefore, a more in-depth discussion is needed to clarify the individual and combined influences of linear and nonlinear components on the propagation effects of femtosecond laser pulses.

In this study, we numerically investigate the spatio-temporal and spectral properties of the linear chirp (LC), quadratic chirp (QC), and the combined linear and quadratic chirps (L-QC) pulses under the collective influence of the diffraction, GVD, SF, and SPM effects. Moreover, the temporal phases and chirps of the three chirped pulses are shown to reveal the mechanisms of temporal distribution changes. And we clarify the role of linear and nonlinear components in the complex chirps by comparing the intensity and spectrum of l-QC with LC and QC pulses. In this paper we focus on QC in complex chirp and cubic nonlinear Kerr effects in medium, without considering higher order chirp or nonlinear

effects. Despite this limitation, our study could contribute to the fundamental research on the nonlinear transmission characteristics of the high-power chirped pulses, and provides valuable theoretical insights for powerful laser experiments and applications.

2. Theoretical model

The evolution of the complex amplitude E(r, t, z) of a chirped pulse propagating along the z-axis in a nonlinear dispersive medium is governed by the nonlinear Schrödinger (NLS) equation. Under the standard paraxial approximation (i.e., $r^2 \ll z^2$) and the slowly varying envelope (i. e., $|\partial^2 E/\partial z^2| \ll |k\partial E/\partial z|$), the NLS equation is expressed as [29]:

$$2ik\frac{\partial E}{\partial z} + \nabla_{\perp}^{2}E - k\beta_{2}\frac{\partial^{2}E}{\partial t^{2}} + 2k^{2}\frac{n_{2}}{n_{0}}|E|^{2}E = 0, \tag{1}$$

where the second and third terms account for the linear diffraction and the GVD effects, respectively, while the fourth term represents both the nonlinear SF (for $n_2>0$) and SPM effects. $\nabla_{\perp}^2=\partial^2/\partial r^2+(1/r)\partial/\partial r$ is the Laplace operator, β_2 is the GVD parameter ($\beta_2>0$ and $\beta_2<0$ corresponding to normal and anomalous GVD, respectively), n_2 and n_0 are the nonlinear and linear refractive indices, respectively, and k is the wave number related to the wavelength λ by $k=2\pi n_0/\lambda$.

Initial field of the chirped pulse is expressed as follows [25]:

$$E(r,t,z=0) = \sqrt{\frac{2P}{\pi w_0^2}} \exp\left(-\frac{r^2}{w_0^2}\right) \times \exp\left(-\frac{t^2}{t_0^2}\right) \exp[-\mathrm{i}\phi_0(t)], \tag{2}$$

where P is the peak beam power, w_0 is the initial beam width, t_0 is the initial pulse width, and $\phi_0(t)$ is the initial chirp phase. The initial linear chirp (LC), quadratic chirp (QC), and linear-quadratic chirp (L-QC) phase are expressed as follows [43]:

$$\phi_{L}(t) = S_{1}t^{2}/t_{0}^{2},
\phi_{Q}(t) = S_{2}t^{3}/t_{0}^{3},
\phi_{L-Q}(t) = S_{3}t^{2}/t_{0}^{2} + S_{4}t^{3}/t_{0}^{3}.$$
(3)

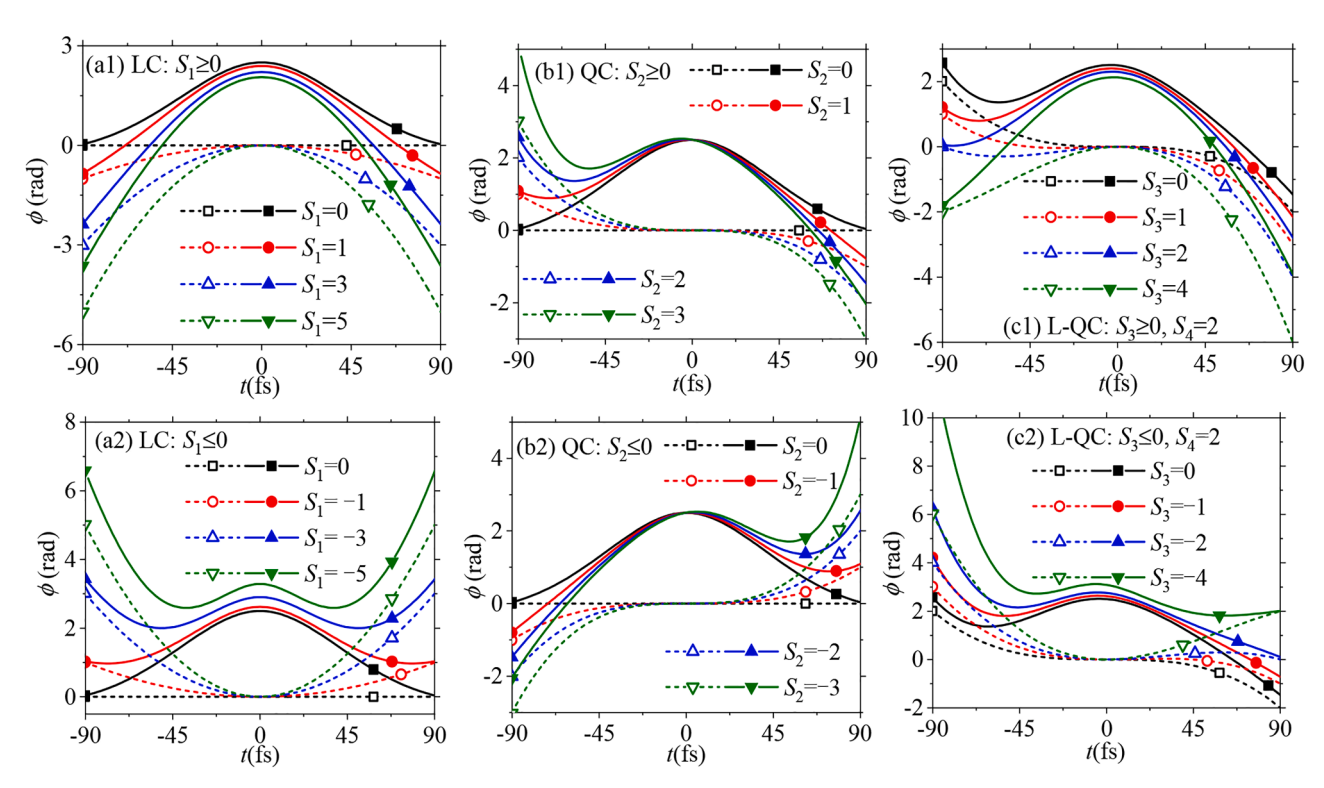


Fig. 2. Temporal phase ϕ distributions of (a) LC, (b) QC, and (c) l-QC pulses at the center of z_1 and z_2 faces; dotted curve: z_1 face, solid curve: z_2 face, $S_4 = 2$.

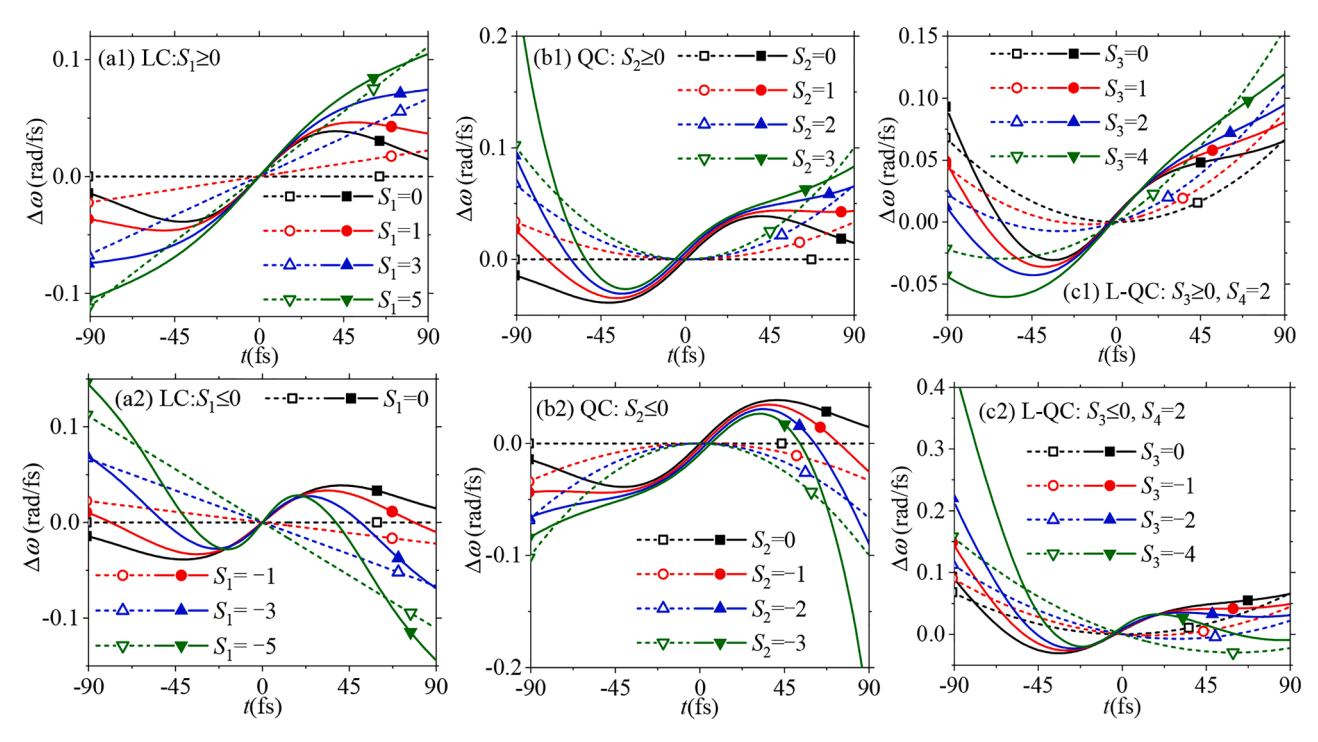


Fig. 3. Chirps $\Delta \omega$ of (a) LC, (b) QC, and (c) l-QC pulses at the center of z_1 and z_2 faces; dotted curve: z_1 face, solid curve: z_2 face, $S_4 = 2$.

The Eq. (1) could be solved numerically via the split-step method [52], the fundamental concept of which is illustrated in Fig. 1. The pulse is transmitted from z to $z+\Delta z$, the linear effects (LE) and nonlinear effects (NE) on the beam within the Δz distance will be calculated separately. The phase modulation resulting from the nonlinear effects is incorporated into the $E(z+\Delta z/2)$ field, and the Crank–Nicholson method [52] is employed for linear transmission calculations both prior to and following the $E(z+\Delta z/2)$ field over a transmission distance of $\Delta z/2$. This numerical calculation enables the generation of field data at transmission position z, encompassing temporal, lateral spatial and spectral dimensions. And it should be noted that the smaller the value of Δz , the more accurate the resulting calculation.

For the calculations, the parameters of the initial pulse are w_0 =70 µm, t_0 =90 fs, λ =800 nm, and P=5 $P_{\rm Cr}$ unless otherwise stated, $P_{\rm Cr}=\lambda^2/(2\pi n_0 n_2)\approx 2.2\times 10^6$ W is the SF critical power of the pulse in fused silica [53], which is used as the normalization factor for the peak beam power. The collapse distance of unchirped pulses is for P=5 $P_{\rm Cr}$ [54]. The parameters of fused silica as the nonlinear dispersive medium are n_0 =1.453, n_2 =3.2 \times 10⁻²⁰ m²/W, β_2 =3.61 \times 10⁻²⁶ s²/m [53], and propagation distance z=6 mm.

3. Effect of initial chirp on temporal phase and chirp

The temporal phases ϕ of LC, QC, and l-QC pulses at the center of z_1 =0 mm and z_2 =6 mm are shown in Figs. 2(a), 2(b), and 2(c), respectively. In these figures, dashed lines represent the phases at z_1 , while solid lines correspond to z_2 , with all figures in this section adhering to this convention. The phase shift $\Delta \phi = \phi(z_2) - \phi(z_1)$ of these chirped pulses illustrated in Fig. 2 is caused by the SPM and GVD effects in medium, which is proportional to the intensity $|E(t)|^2$. Thus the maximum phase shift $(\Delta \phi)_{\rm max}$ of LC pulse occurs at t=0, while shift from t=0 for QC and l-QC pulses due to temporal asymmetric intensity (as illustrated in Figs. 5 and 8). Notably, the initial chirps with different types and values influence the $(\Delta \phi)_{\rm max}$ in significantly different ways. As shown in Figs. 2(a1) and 2(c1), the positive LC parameters (S_1 and S_3) are larger, the pulse stretching is faster, the SPM effect is weaker, and the $(\Delta \phi)_{\rm max}$ are smaller. While as the value of the negative LC parameters (S_1 and S_3) increases in Figs. 2(a2) and 2(c2), the pulse compression is

faster, the SPM effect is enhanced, and the $(\Delta\phi)_{\rm max}$ are larger. Moreover, Figs. 2(b1) and 2(b2) indicate that the $(\Delta\phi)_{\rm max}$ of the QC pulses for positive and negative chirp parameters are equal as the absolute value of chirp parameters is same, due to the values of peak intensity $(|E(t)|^2)_{\rm max}$ are equal as $S_2(S_2>0)=|S_2|(S_2<0)$ (as illustrated in Fig. 5).

Differentiating phase $\phi(r, t, z)$ with respect to t, we obtain the chirp of pulse in propagation [25]:

$$\Delta\omega(r,t,z) = -\partial\phi(r,t,z) / \partial t. \tag{4}$$

The difference from the center frequency indicates that the pulse with a low frequency at the front and high frequency at the back is called positive chirp pulse, while the reverse scenario signifies a negative chirp

The chirps $\Delta \omega$ of LC, QC, and l-QC pulses at the center of z_1 and z_2 are depicted in Figs. 3(a), 3(b), and 3(c), respectively. The initial nonlinear chirp distributions reveal that a sequence from negative to positive chirp occurs in the pulse as the QC parameters $S_2>0$ (as shown in Fig. 3(b1)) and $S_4>0$ (as shown in Figs. 3(c1) and 3(c2)), with the reverse sequence occurring when S_2 <0 (as illustrated in Figs. 3(b2)) and S_4 <0 (graphics omitted here to save space). And the LC parameter S_3 in 1-QC pulses can modulate the duration and magnitude of the initial positive and negative chirps (as shown in Fig. 3(c)). Moreover, the output chirps are nonlinear due to the SPM effect during propagation, with positive chirps always present within the pulse center range (the results are in agreement with those in reference [25], which studied the chirp distribution of the linearly chirped pulse in propagation with the Kerr effect), i.e., the initial negative chirps change to output positive chirps, which is the reason why the output spectra with initial negative chirps are narrower than that with initial positive chirps (as illustrated in Fig. 10). Additionally, the output positive chirp duration significantly responds to the chirp parameters, which increases as QC and positive LC parameters increase with the stronger positive chirp effect (as illustrated in Figs. 3(a1), 3(b) and 3(c1)), and decreases as negative LC parameter value increases with the stronger negative chirp effect (as illustrated in Figs. 3(a2) and 3(c2)).

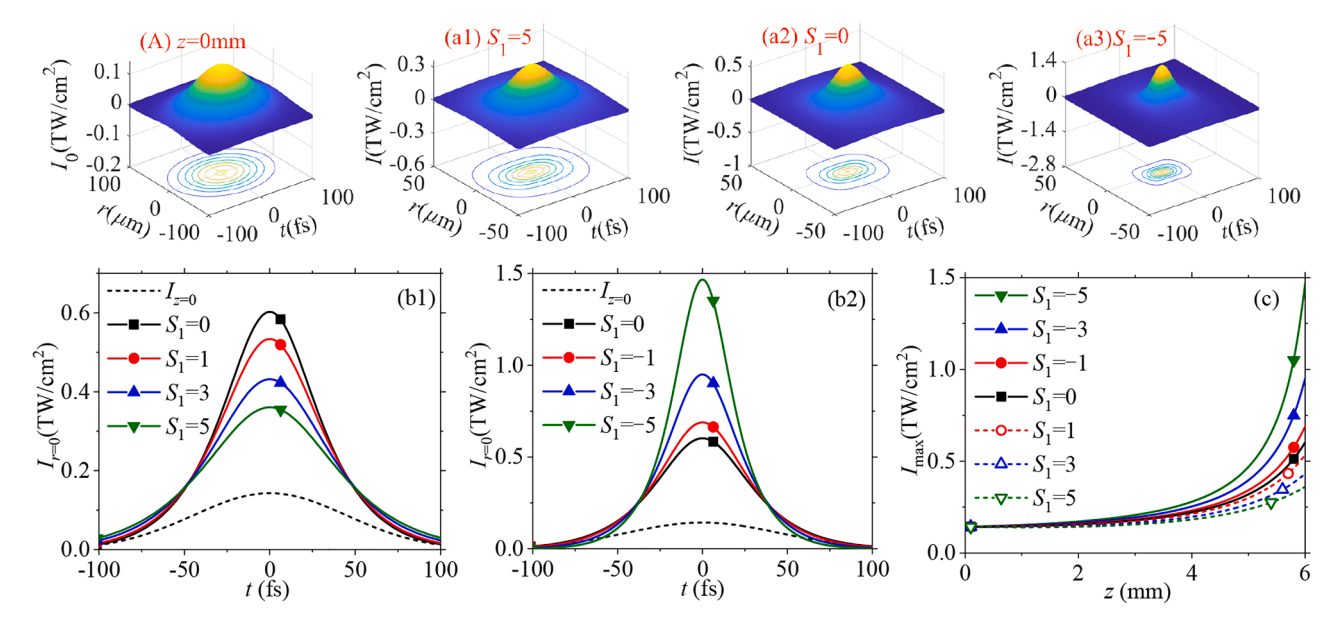


Fig. 4. (A) Initial intensity of both unchirped and chirped pulses. For LC pulses, (a) intensity and its contour distributions at the z_2 face; (b) on-axis intensity distributions at the z_2 face; (c) the peak intensities I_{max} versus the propagation distance z.

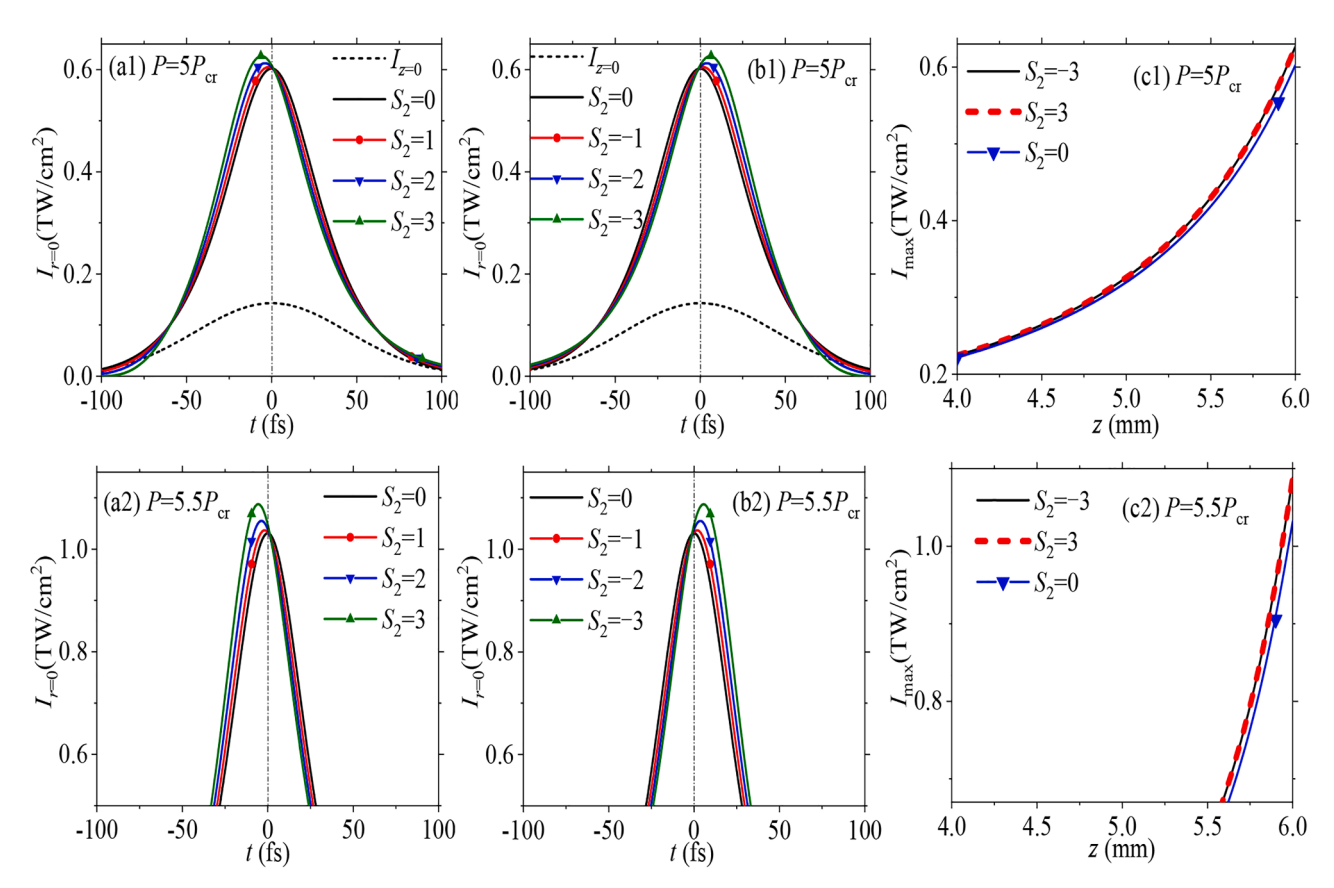


Fig. 5. For QC pulses, (a) and (b) on-axis intensity distributions at the z_2 face; (c) the peak intensities I_{max} versus the propagation distance z.

4. Effect of initial chirp on intensity distributions

4.1. Effect of individual initial LC and QC

The initial intensity and its contour distributions for both unchirped and chirped pulses, as a reference, is shown in Fig. 4(A). For the LC pulses, the intensity distributions at the z_2 face, and the changes of the

peak intensities $I_{\rm max}$ versus the propagation distance z are presented in Figs. 4(a–b) and 4(c), respectively. The results indicate that with positive chirp ($S_1>0$), as S_1 increases, the pulse width during propagation is broadened by the GVD effect, leading to a weaker spatial SF effect under smaller intensity and an increase in beam width. Similarly, the pulse width increases and intensity decreases as S_1 increases in linear propagation [35–41]. Conversely, the scenario is reversed when $S_1<0$.

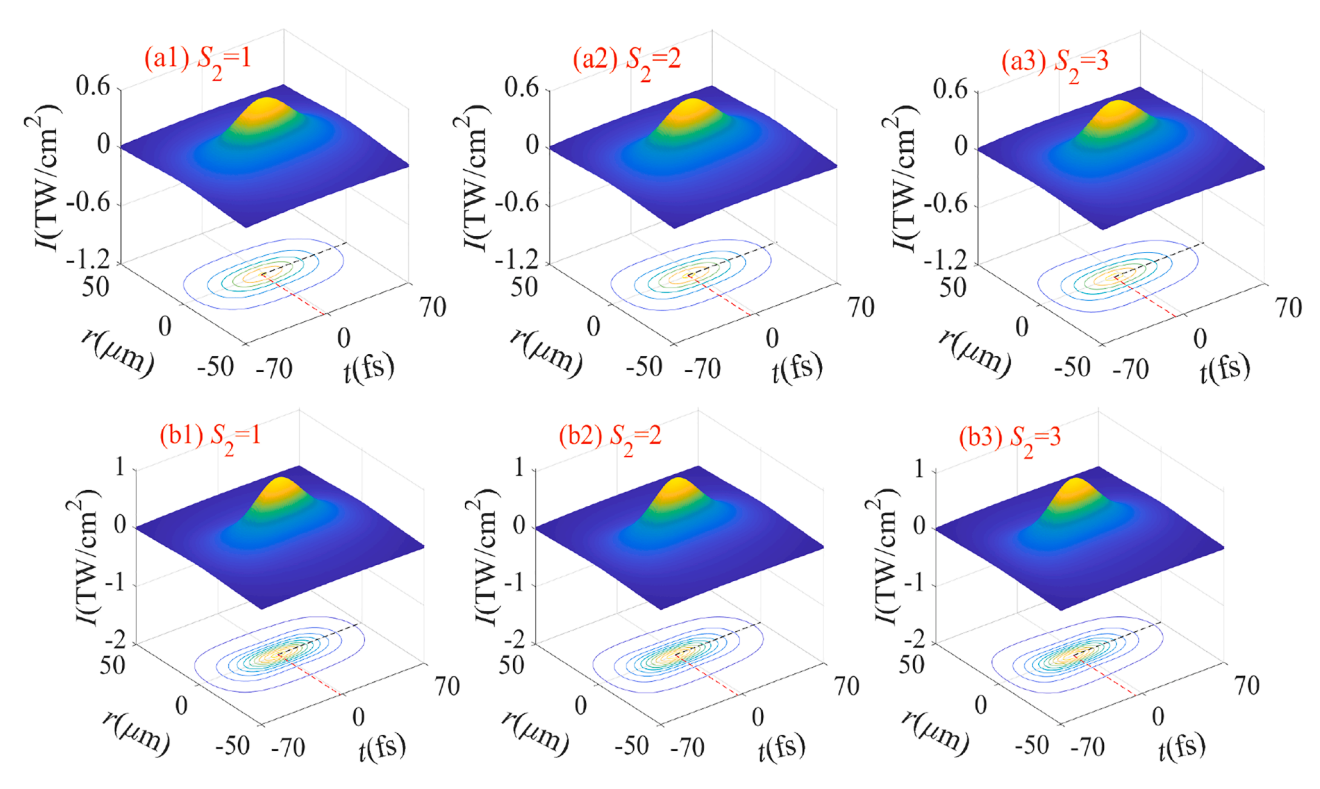


Fig. 6. Intensity and its contour distributions of QC pulses at the z_2 face; (a) P = 5 $P_{\rm cr}$, (b) P = 5.5 $P_{\rm cr}$

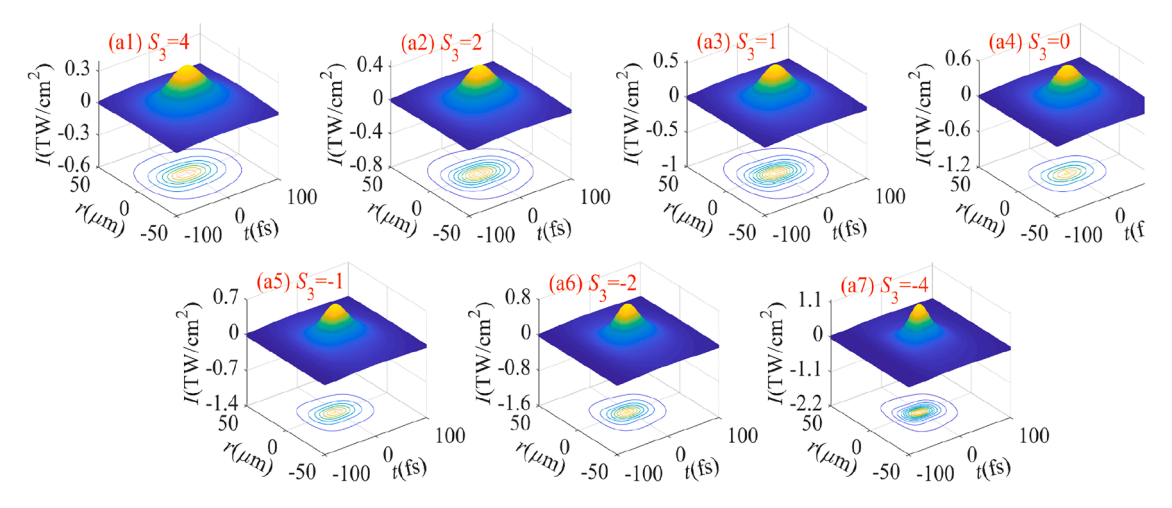


Fig. 7. Intensity and its contour distributions of l-QC pulses at the z_2 face, S_4 =2.

The on-axis intensity distributions of the QC pulse at the z_2 face are illustrated in Figs. 5(a) and 5(b). For $S_2>0$, as shown in Fig. 5(a), the peak intensity of the pulse occurs earlier than at the t=0 moment. This phenomenon results from the negative chirp at the pulse's front edge causing compression, while the positive chirp at the trailing edge leads to broadening. Conversely, for $S_2 < 0$, as depicted in Fig. 5(b), the situation is reversed. It is worth mentioning that the time shift of the peak intensity of the QC pulse also occurs in linear transmission [43]. Notably, an increase in $|S_2|$ enhances the peak intensity, attributed to the larger value of the negative chirp component in QC and more pulse compression. Additionally, the changes of the peak intensities I_{max} of the QC pulse versus the propagation distance z are shown in Fig. 5(c), showing that the positive and negative QCs with the same absolute value enhance the peak intensity by the same amount during propagation. Specifically, as the power increases, the effect of the QC on enhancing the peak intensity becomes stronger, this conclusion is obtained by

comparing Figs. 5(a1) with 5(a2), Figs. 5(b1) with 5(b2), and Figs. 5(c1) with 5(c2) with the same coordinate dimensions.

Furthermore, the intensity and its contour distributions of the QC pulses at the z_2 face for P=5 $P_{\rm cr}$ and P=5.5 $P_{\rm cr}$ (with $L_{\rm SF}=13.2$ mm) are presented in Figs. 6(a) and 6(b), respectively. These figures reveal that the temporal intensity distributions shift forward for $S_2>0$, while the spatial intensity distributions remain symmetric about r=0, due to the spatial diffraction and SF effect are always symmetrical. For $S_2<0$, the temporal shift is reversed which is predictable and omitted here.

4.2. Effect of initial l-QC

The intensity and contour distributions of the l-QC pulses at the z_2 face for different LC parameters S_3 , with the QC parameter set to S_4 =2, are depicted in Fig. 7. These figures demonstrate that for S_3 >0, as S_3 increases, the temporal pulse spreading increases and the spatial SF

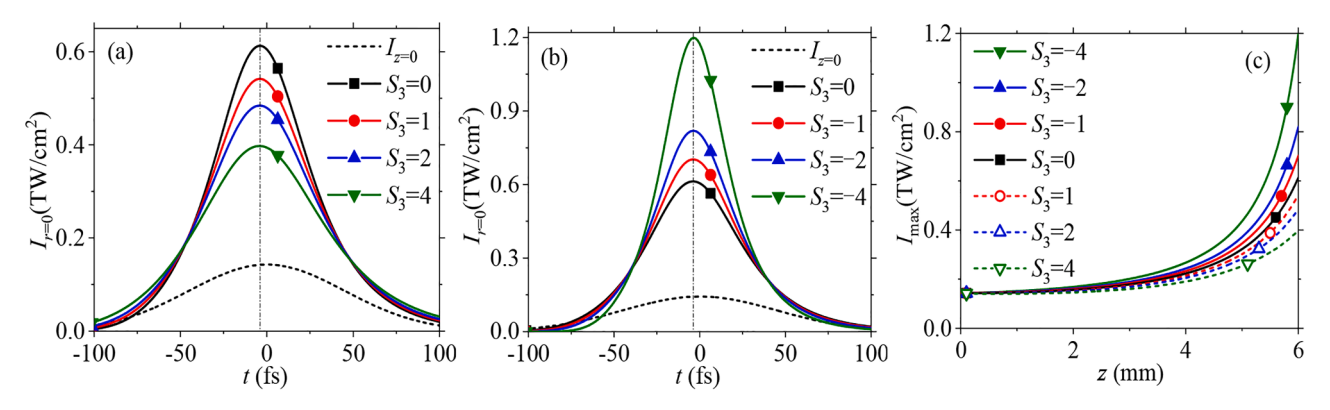


Fig. 8. For l-QC pulses, (a) and (b) on-axis intensity distributions of l-QC pulse at the z_2 face; (c) the peak intensities $I_{\rm max}$ versus the propagation distance z, $S_4=2$.

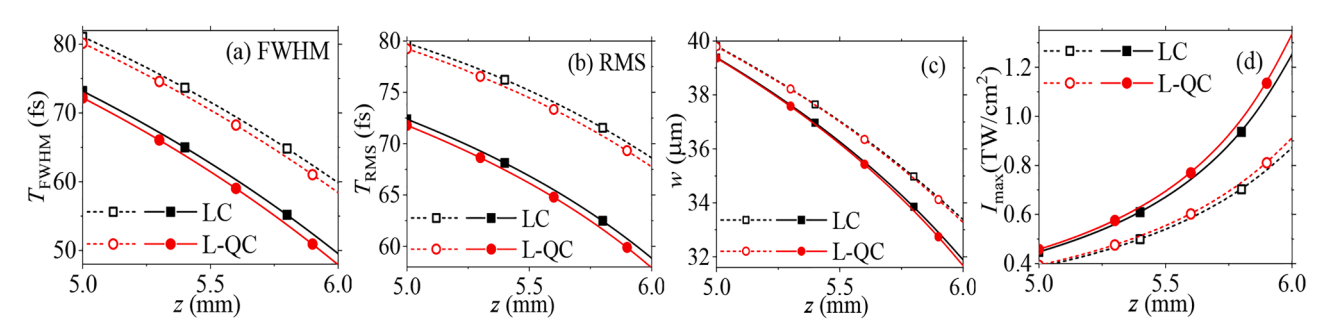


Fig. 9. The changes of the full pulse width (a) T_{FWHM} and (b) T_{RMS} , (c) the mean-squared beam width w, and (d) the peak intensities I_{max} of LC and l-QC pulses versus the propagation distance z; solid lines: $S_1 = S_3 = -1$, dashed lines: $S_1 = S_3 = 1$, $S_4 = 3$, $P_5 = 5$. P_{CL} .

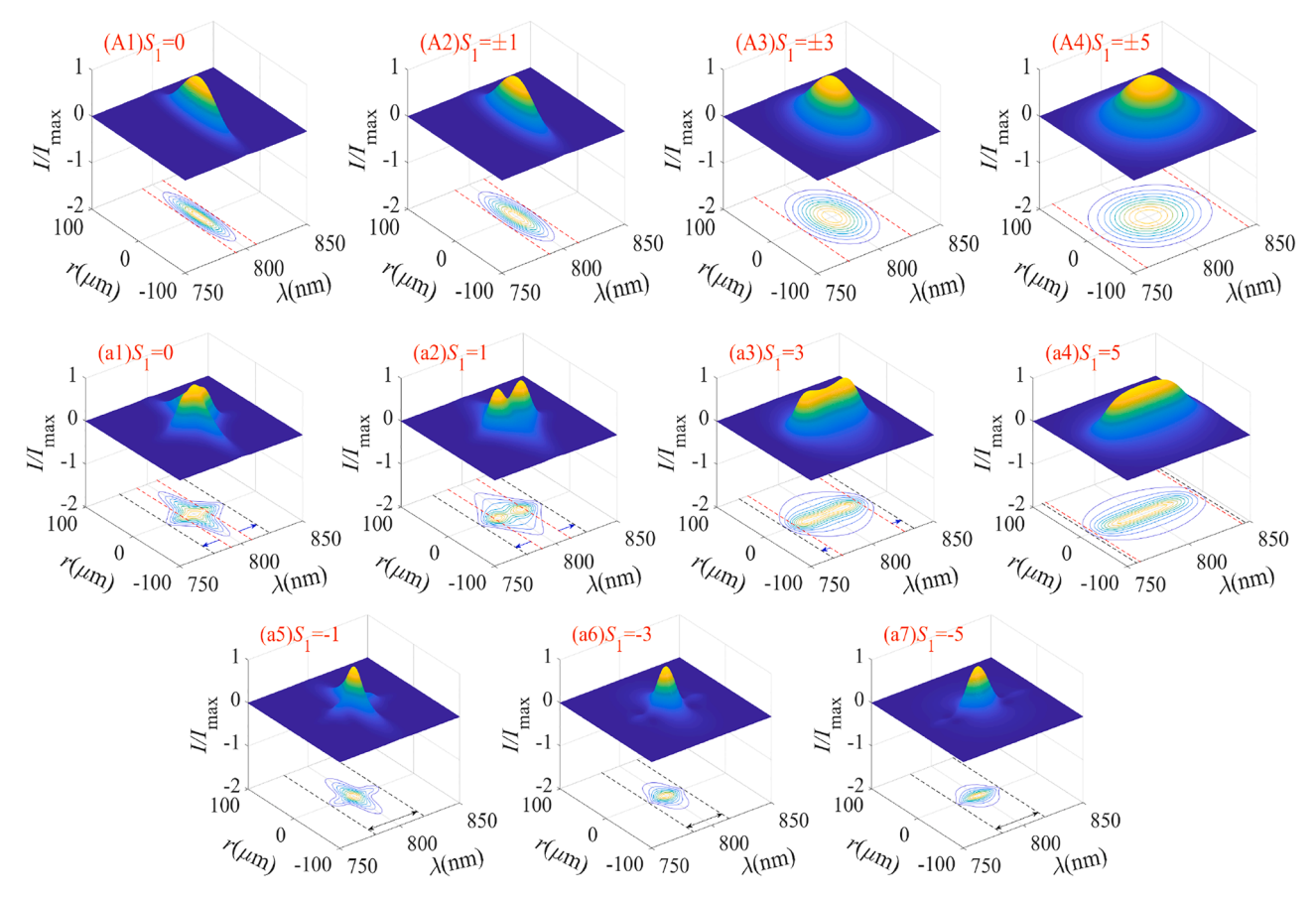


Fig. 10. Spectrum and its contour distributions of LC pulses, at (A) z_1 face and (a) z_2 face.

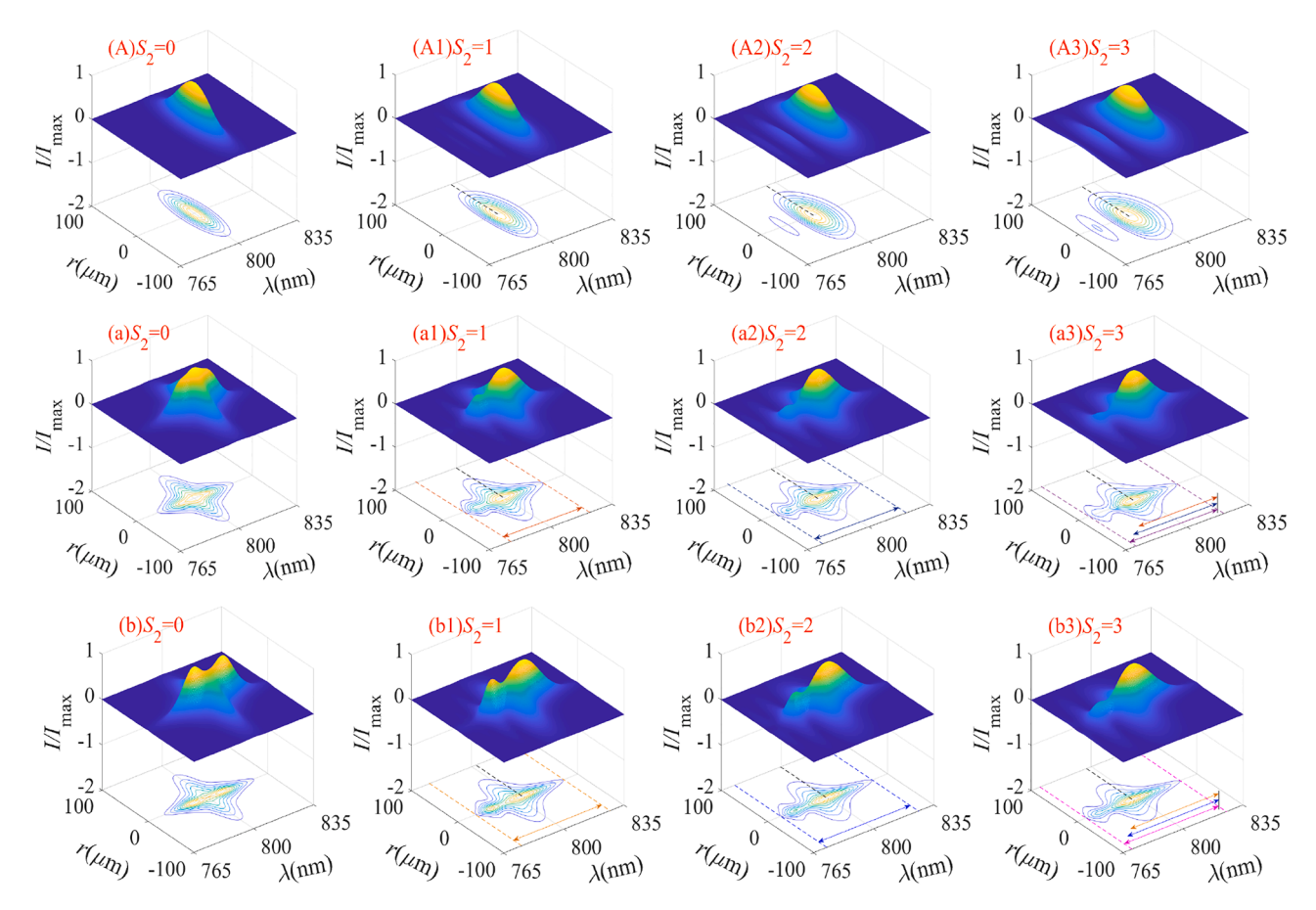


Fig. 11. Spectrum and its contour distributions of QC pulses; (A) P = 5 P_{cr} and P = 5.5 P_{cr} at z_1 face, (a) P = 5 P_{cr} at z_2 face, (b) P = 5.5 P_{cr} at z_2 face.

effect weakens, resulting in a more diffuse intensity distribution and a lower peak intensity. Conversely, as $|S_3|$ increases with $S_3 < 0$, the temporal pulse compression increases and the spatial SF effect strengthens, leading to a more compact intensity distribution and a higher peak intensity. Additionally, the effects of LC parameters on intensity distributions in both LC and l-QC pulses are observed to be similar.

The on-axis intensity distributions depicted in Fig. 7 (i.e., at r=0) are further illustrated in Figs. 8(a) and 8(b). The QC in the l-QC pulse influences the latency time of the pulse's peak intensity. The peak intensity occurs earlier than the t=0 moment when $S_4>0$ ($S_4=2$), while it is delayed when $S_4<0$, a behavior that is independent of the LC parameter S_3 . Furthermore, the effects of QC parameters on the latency time of peak intensity are consistent between QC and l-QC pulses. Additionally, the changes of the peak intensities $I_{\rm max}$ of the l-QC pulses versus the propagation distance z are shown in Fig. 8(c). The figure shows that the $I_{\rm max}$ of the l-QC pulses with negative LC are always greater than those with positive LC and only QC during the entire propagation, due to the pulse compression and stronger SF effect caused by the negative chirp.

The changes of the full pulse width $T_{\rm FWHM}$ and $T_{\rm RMS}$ at r=0, the mean-squared beam width w at temporal maximum intensity, and the peak intensities $I_{\rm max}$ of LC and l-QC pulses versus the propagation distance z are shown in Fig. 9. The $T_{\rm FWHM}$ and $T_{\rm RMS}$ are defined by the full width at half maximum (FWHM) and the root-mean-square (RMS) [55], respectively. The solid lines and dashed lines represent the negative $(S_1{=}S_3{=}{-}1)$ and positive $(S_1{=}S_3{=}1)$ LC parameters of LC and l-QC pulses, respectively, and the QC parameter of l-QC pulses set to $S_4{=}3$. These figures demonstrate that, for both the positive and negative LC pulses, the introduced QC could further compress the pulse's spatio-temporal distributions, i.e., decrease the pulse width and beam width of the pulse, and increase the peak intensities.

5. Effect of initial chirp on spectrum distributions

5.1. Effect of initial LC

The spectrum and its contour distributions of the LC pulses at the z_1 and z_2 faces are illustrated in Figs. 10(A) and 10(a), respectively. For $S_1>0$, the SPM effect in the medium causes the spectral broadening during propagation. As S_1 increases, the SPM effect weakens, the spectral broadening decreases (as indicated by the distance between the red and black auxiliary lines in Figs. 10(a1-a4)), but the output spectral width increases owing to the wider initial spectrum. For $S_1 < 0$, the spectral chirp induced by the SPM effect is opposite to the initial chirp within the pulse center range with majority of pulse energy (as shown in Fig. 3(a2)), thus the output spectral width with $S_1 < 0$ is narrower than that with $S_1>0$. Additionally, the narrower spatial width of the spectra in Figs. 10(a5-a7), comparing to that in Figs. 10(a2-a4), demonstrates that the SF effect is stronger when $S_1 < 0$. Moreover, the multiple peaks in output spectra result from the interference of beams with the same frequency and different phases which is caused by the SPM effect in medium (as shown in Figs. 2 and 3). And the claim apply to the spectra both of linear and nonlinear chirp pulses.

5.2. Effect of initial QC

The spectrum and contour distributions of the QC pulses at the z_1 and z_2 faces for $S_2>0$ are depicted in Figs. 11(A) and 11(a–b), respectively. For both initial and output spectra, the wavelengths with maximum intensity become smaller as $|S_2|$ increases (as indicated by the short dotted lines in Fig. 11), and the spectral side lobes are all in short wavelength direction, which echoes the frequency distributions shown in figure 3(b1). Moreover, the output spectral width increases as $|S_2|$ or

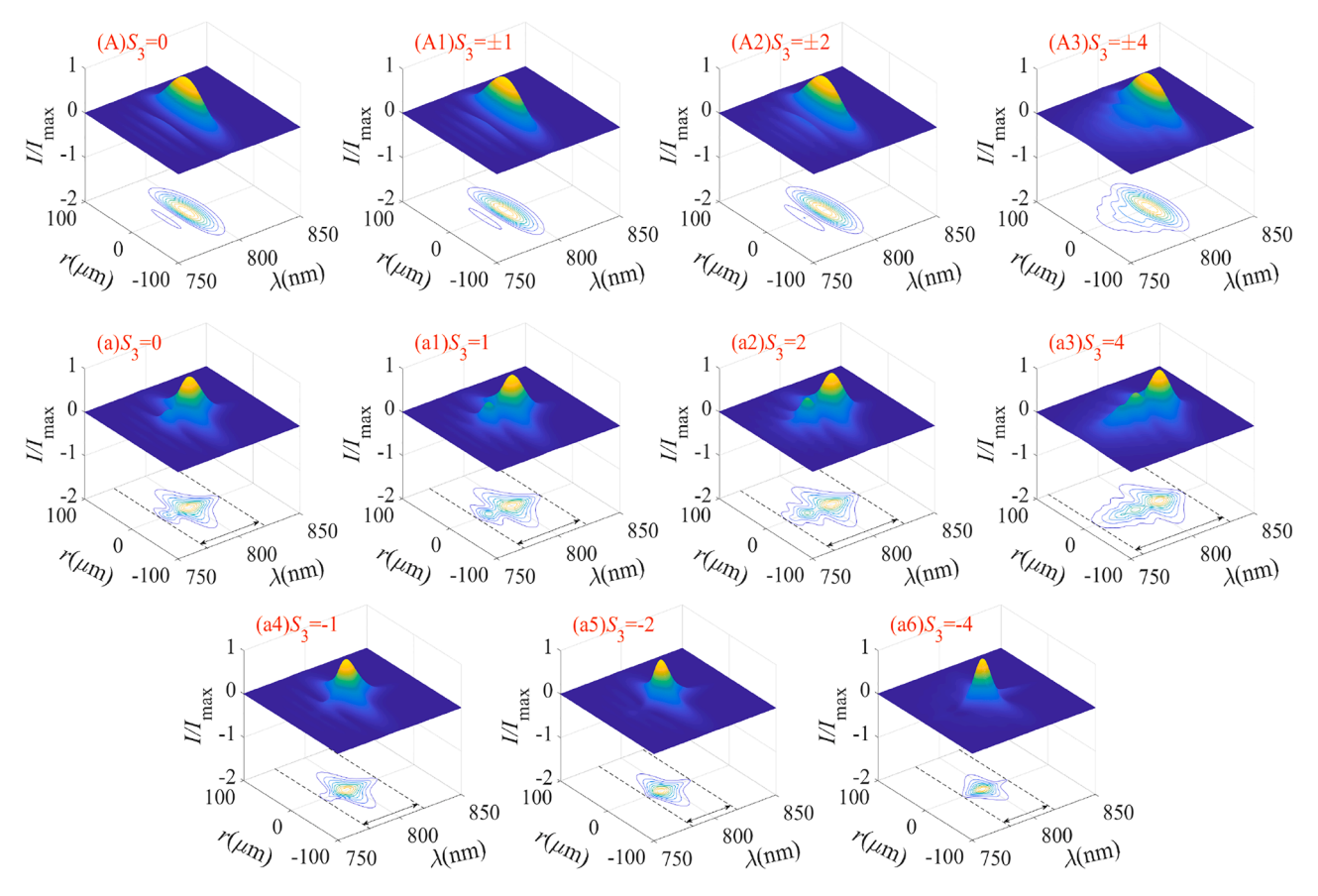


Fig. 12. Spectrum and its contour distributions of l-QC pulses, at (A) z_1 face and (a) z_2 face, S_4 =2.

the power increases with the wider initial spectrum or stronger SPM effect in medium (as indicated by the double arrow lines in Figs. 11(a) and 11(b)). Specifically, the spectrum distributions at both z_1 and z_2 faces for $S_2{>}0$ and $S_2{<}0$, with the same value, are symmetric about the central wavelength of 800 nm, and the cases of $S_2{<}0$ are omitted here to save space.

5.3. Effect of initial l-QC

The spectrum and contour distributions of the l-QC pulses at the z_1 and z_2 faces for different LC parameters S_3 , with S_4 =2, are presented in Figs. 12(A) and 12(a), respectively. The figures reveal that the spectrum distributions for $S_3>0$ and $S_3<0$, with the same value, are identical at the z_1 face but differ at the z_2 face. The underlying reason for this is that the wavelength (or frequency) components of the pulse at the z_1 face are the same, while the distribution of frequency (or chirp) with time varies. The spectrum distributions of the L–QC pulses at the z_2 face, especially for $S_3>0$, differ from those of the LC pulses (as shown in Fig. 10(a)) when QC is introduced. For $S_3>0$, the output spectra exhibit multiple side lobes due to multiple side lobes in the initial spectra, and the SPM effect mainly enables the spectral broadening with positive chirp. Moreover, as S_3 increases, both the initial and output spectra are wider. Conversely, for $S_3 < 0$, an increase in $|S_3|$ enhances the SPM effect, and the output spectrum is narrower, this is due to the fact that the spectral chirp introduced by the SPM effect is opposite to the initial negative chirp within the pulse center range with majority of pulse energy (as shown in Fig. 3(c2)). Additionally, the LC parameter has a similar effect on spectrum distributions in both LC and 1-QC pulses. In addition, it is shown that, in comparison with the spectral distributions of QC pulses in Fig. 11, the LC component in l-QC pulses could modulate both spectral broadening and narrowing, exhibiting heightened sensitivity.

6. Conclusion

In summary, our numerical investigation has focused on the propagation properties of LC, QC, and l-QC pulses in a nonlinear medium. We have demonstrated the distinct effects of these three types of chirps on the spatio-temporal and spectral properties of pulses, their temporal phase and chirp during propagation, and the nonlinear effects within the medium. It is shown that the LC and QC in l-QC pulse play different roles in modulating the intensity and spectrum of pulse. On the one hand, the QC of pulse causes a notable shift of the peak intensity from the t =0 moment, which is independent of the LC, and the introduction of QC in conjunction with LC leads to a further compression of the pulse's spatiotemporal distribution and an increase in intensity. Moreover, the effects of QC in both QC and l-QC pulses are enhanced as the power increases. On the other hand, spectral broadening and narrowing are more sensitive to LC than to QC. Thus we can know that the l-QC pulses are more operational in modulating intensity and spectral distribution of pulse. Furthermore, our research findings may be validated through the utilization of AODDL, the autocorrelation [56] and spectrometer, which will be the subsequent phase of our investigation. And in addition to the temporal chirps, the specific spatial configurations of the beams and the modulation of the wavefront have a profound impact on the transmission characteristics of the pulses, which require further investigation.

CRediT authorship contribution statement

Jing Hu: Writing – review & editing, Writing – original draft, Validation, Investigation. **Lihe Yan:** Writing – review & editing, Supervision. **Jinhai Si:** Supervision. **Qinjun Jian:** Formal analysis. **Xun Hou:** Supervision.

Declaration of competing interest

The authors declare that they have no known competing financial interests or personal relationships that could have appeared to influence the work reported in this paper.

Acknowledgments

This work was supported by the National Natural Science Foundation of China (Grant No. 62027822) and the National R&D Program of China (Grant No. 2019YFA0706402).

Data availability

No data was used for the research described in the article.

References

- [1] Y. Yalikun, Y. Hosokawa, T. Iino, Y. Tanaka, An all-glass 12 µm ultra-thin and flexible micro-fluidic chip fabricated by femtosecond laser processing, Lab Chip 16 (2016) 2427.
- [2] B. Xu, Y. Shi, Z. Lao, J. Ni, G. Li, Y. Hu, J. Li, J. Chu, D. Wu, K. Sugioka, Real-time two-photon lithography in controlled flow to create a single-microparticle array and particle-cluster array for optofluidic imaging, Lab Chip 18 (2018) 442.
- N. Liu, Y. Sun, H. Wang, C. Liang, Femtosecond laser-induced nanostructures on Fe-30Mn surfaces for biomedical applications, Opt. Laser Technol. 139 (2021) 106986
- [4] J. Zheng, X. Zhang, Y. Zhang, F. Yuan, Osteoblast differentiation of bone marrow stromal cells by femtosecond laser bone ablation, Biomed. Opt. Express 11 (2020)
- [5] I. Dicaire, V. Jukna, C. Praz, C. Milián, L. Summerer, A. Couairon, Spaceborne laser filamentation for atmospheric remote sensing, Laser Photonics Rev 10 (2016) 481.
- H.L. Xu, S.L. Chin, Femtosecond laser filamentation for atmospheric sensing, Sensors 11 (2011) 32.
- [7] C.P. Jisha, J. Beeckman, F.V. Acker, K. Neyts, S. Nolte, A. Alberucci, Generation of multiple solitons using competing nonlocal nonlinearities, Opt. Lett 44 (2019)
- [8] A.C.A. Siqueira, E.L. Falcão-Filho, B.A. Malomed, C.B. de Araújo, Generation of multiple ultrashort temporal solitons in a third-order nonlinear composite medium with self-focusing and self-defocusing nonlinearities, Phys. Rev. A 107 (2023) 063519.
- [9] I. Towers, B.A. Malomed, Stable (2+1)-dimensional solitons in a layered medium with sign-alternating Kerr nonlinearity, J. Opt. Soc. Am. B 19 (2002) 537.
- [10] A.H. Arnous, A. Biswas, A.H. Kara, Y. Yıldırım, L. Moraru, C. Iticescu, S. Moldovanu, A.A. Alghamdi, Optical solitons and conservation laws for the concatenation model with spatio-temporal dispersion (internet traffic regulation), in: J. Eur. Opt. Society-Rapid Publ, 19, 2023, p. 35.
- [11] Y. Yildirim, Optical solitons to Biswas-Arshed model in birefringent fibers using modified simple equation architecture, Optik (Stuttg) 182 (2019) 1149.
- [12] Y. Yıldırım, Sub pico-second pulses in mono-mode optical fibers with Triki-Biswas model using trial equation architecture, Optik (Stuttg) 183 (2019) 463.
- Y. Yildirim, Bright, dark and singular optical solitons to Kundu-Eckhaus equation having four-wave mixing in the context of birefringent fibers by using of modified simple equation methodology, Optik (Stuttg) 182 (2019) 110.
- [14] Y. Yildirim, Optical solitons of Biswas-Arshed equation by modified simple quation technique, Optik (Stuttg) 182 (2019) 986.
- [15] Y. Yildirim, Optical solitons of Biswas-Arshed equation in birefringent fibers by trial equation technique, Optik (Stuttg) 182 (2019) 810.
- [16] A.H. Arnous, A. Biswas, Y. Yildirim, L. Moraru, C. Iticescu, L.G. Puiu, A. Asiri, Optical solitons and complexitons for the concatenation model in birefringent fibers, Ukr. J. Phys. Opt. 24 (2023) 4060.
- [17] N.A. Kudryashov, A. Biswas, A.G. Borodina, Y. Yıldırım, H.M. Alshehri, Painlevé analysis and optical solitons for a concatenated model, Optik (Stuttg) 272 (2023)
- [18] Y. Yıldırım, A. Biswas, M. Ekici, H. Triki, O. Gonzalez-Gaxiola, A.K. Alzahrani, M. R. Belic, Optical solitons in birefringent fibers for Radhakrishnan-Kundu-Lakshmanan equation with five prolific integration norms, Optik (Stuttg) 208 (2020) 164550.
- [19] A. Darwish, E.A. El-Dahab, H. Ahmed, A.H. Arnous, M.S. Ahmed, A. Biswas, P. Guggilla, Y. Yıldırım, F. Mallawi, M.R. Belic, Optical solitons in fiber Bragg gratings via modified simple equation, Optik (Stuttg) 203 (2020) 163886.
- [20] J. Kasparian, M. Rodriguez, G. Méjean, J. Yu, E. Salmon, H. Wille, R. Bourayou, S. Frey, Y.-B. André, A. Mysyrowicz, R. Sauerbrey, J.-P. Wolf, L. Wöste, White-light filaments for atmospheric analysis, Science 301 (2003) 61.
- [21] H. Xu, Y. Cheng, S.L. Chin, H.B. Sun, Femtosecond laser ionization and fragmentation of molecules for environmental sensing, Laser Photon. Rev 9 (2015)
- [22] A. Houard, P. Walch, T. Produit, V. Moreno, B. Mahieu, A. Sunjerga, C. Herkommer, A. Mostajabi, U. Andral, Y.-B. André, M. Lozano, L. Bizet, M. C. Schroeder, G. Schimmel, M. Moret, M. Stanley, W.A. Rison, O. Maurice,

- B. Esmiller, K. Michel, W. Haas, T. Metzger, M. Rubinstein, F. Rachidi, V. Cooray, A. Mysyrowicz, J. Kasparian, J.P. Wolf, Laser-guided lightning, Nat. Photon. 17 (2023) 231.
- [23] C.L. Arnold, C.J. Saraceno, M.T.C. de Barros, Lightning protection by laser, Nat. Photon. 17 (2023) 211.
- [24] G.L. Roth, C. Esen, R. Hellmann, Femtosecond laser direct generation of 3Dmicrofluidic channels inside bulk PMMA, Opt. Express 25 (2017) 18442.
- [25] G. Zhang, X. Ji, Chirp characteristics and the effect of chirp on the beam quality of laser pulses propagating upwards in the atmosphere, Phys. Scr. 98 (2023) 065522.
- [26] Y. Zhang, X. Ji, H. Zhang, X. Li, T. Wang, Self-focusing and group-velocity dispersion of pulsed laser beams in the inhomogeneous atmosphere, Opt. Express 26 (2018) 14617.
- [27] D. Strickland, G. Mourou, Compression of amplified chirped optical pulses, Opt. Commun 55 (1985) 447.
- A.Goyal Alka, R. Gupta, C.N. Kumar, T.S. Raju, Chirped femtosecond solitons and double-kink solitons in the cubic-quintic nonlinear Schrödinger equation with selfsteepening and self-frequency shift, Phys. Rev. A 84 (2011) 063830.
- [29] V. Kartazaev, R.R. Alfano, Supercontinuum generated in calcite with chirped femtosecond pulses, Opt. Lett. 32 (2007) 3293.
- [30] X.D. Cao, G.P. Agrawal, C.J. McKinstrie, Self-focusing of chirped optical pulses in nonlinear dispersive media, Phys. Rev. A 49 (1994) 4085.
- [31] R. Nuter, S. Skupin, L. Bergé, Chirp-induced dynamics of femtosecond filaments in air, Opt. Lett 30 (2005) 917.
- J.R. Peñano, P. Sprangle, B. Hafizi, A. Ting, D.F. Gordon, C.A. Kapetanakos, Propagation of ultra-short, intense laser pulses in air, Phys. Plasmas 11 (2004)
- [33] R. Nuter, S. Skupin, L. Bergé, Self-focusing and group-velocity dispersion of pulsed laser beams in the inhomogeneous atmosphere, Opt. Lett. 30 (2005) 917.
- [34] R. Nuter, L. Bergé, Pulse chirping and ionization of O2 molecules for the filamentation of femtosecond laser pulses in air, J. Opt. Soc. Am. B 23 (2006) 874.
- S.A. Diddams, H.K. Eaton, A.A. Zozulya, T.S. Clement, Amplitude and phase measurements of femtosecond pulse splitting in nonlinear dispersive media, Opt. Lett. 23 (1998) 379.
- [36] H. Pakarzadeh, Z. Delirian, M. Taghizadeh, Simulation of Chirped Pulse Propagation in Silicon Nanowires: shape and Spectrum Analysis, Opt. Photonics Journal 6 (2016) 53.
- [37] L. Ladányi1, L. Scholtz, J. Müllerová, Numerical simulations of dispersion effects in chirped Gaussian and soliton pulses, Opt. Quant. Electron. 49 (2017) 105.
- [38] Z. Zhu, T.G. Brown, Experimental studies of polarization properties of supercontinua generated in a birefringent photonic crystal fiber, Opt. Express 12 (2004) 689.
- [39] K. Beckwitt, F.W. Wise, L. Qian, L.A. Walker, E. Canto-Said, Compensation for selffocusing by use of cascade quadratic nonlinearity, Opt. Lett. 26 (2001) 1696.
- [40] X. Liu, L. Qian, F. Wise, High-energy pulse compression by use of negative phase shifts produced by the cascade χ⁽²⁾:χ⁽²⁾ nonlinearity, Opt. Lett. 24 (1999) 1777.
 [41] L.J. Qian, X. Liu, F.W. Wise, Femtosecond Kerr-lens mode locking with negative
- nonlinear phase shifts, Opt. Lett. 24 (1999) 166.
- [42] X. Shi, X. Huang, Y. Deng, C. Tan, Y. Bai, X. Fu, Dynamic propagation of symmetric Airy pulses with initial chirps in an optical fiber, Opt. Commun. 399 (2017) 16.
- [43] H. Akou, Effect of various chirped frequency functions on Gaussian laser beam characteristics, Optik (Stuttg) 131 (2016) 446.
- S. Afhami, E. Eslami, Effect of nonlinear chirped Gaussian laser pulse on plasma wake field generation, AIP Adv 4 (2014) 087142.
- [45] V.Y. Molchanov, K.B. Yushkov, P.V. Kostryukov, P.B. Gornostaev, N.S. Vorobiev, Measurement of amplified binary-modulated chirped laser pulses generated by different acousto-optic pulse shaping algorithms, Opt. Laser Technol. 142 (2021)
- [46] E.T.J. Nibbering, M.A. Franco, B.S. Prade, G. Grillon, J.P. Chambaret, A. Mysyrowicz, Spectral determination of the amplitude and the phase of intense ultrashort optical pulses, J. Opt. Soc. Am. B 13 (1996) 317.
- [47] M. Oberthaler, R.A. Höpfel, Special narrowing of ultrashort laser pulses by selfphase modulation in optical fibers, Appl. Phys. Lett. 63 (1993) 1017.
- [48] H. Triki, K. Porsezian, A. Choudhuri, P.T. Dinda, Chirped solitary pulses for a nonic nonlinear Schrödinger equation on a continuous-wave background, Phys. Rev. A 93 (2016) 063810.
- [49] H. Triki, V.I. Kruglov, Chirped self-similar solitary waves in optical fibers governed with self-frequency shift and varying parameters, Chaos. Soliton. Fract. 143 (2021)
- [50] H. Triki, B. Wang, Q. Zhou, Controlled linearly chirped similaritons in inhomogeneous birefringent optical fibers, Phys. Lett. A 503 (2024) 129419.
- [51] M. Oberthaler, R.A. Höpfel, Special narrowing of ultrashort laser pulses by selfphase modulation in optical fiber, Appl. Phys. Lett. 63 (1993) 1017.
- A. Couairon, E. Brambilla, T. Corti, D. Majus, O. de J. Ramírez-Góngor M. Kolesik, Practitioner's guide to laser pulse propagation models and simulation, Eur. Phys. J. Spec. Top. 199 (2011) 5.
- S. Tzortzakis, L. Sudrie, M. Franco, B. Prade, A. Mysyrowicz, A. Couairon, L. Bergé, Self-guided propagation of ultrashort IR laser pulses in fused silica, Phys. Rev. Lett. 87 (2001) 213902.
- [54] H. Wang, X.L. Ji, Y. Deng, X.Q. Li, H. Yu, Theory of the quasi-steady-state selffocusing of partially coherent light pulses in nonlinear media, Opt. Lett 45 (2020)
- [55] D. Marcuse, Pulse distortion in single-mode fibers, Appl. Opt. 19 (1980) 1653.
- [56] P. Lassonde, S. Mironov, S. Fourmaux, S. Payeur, E. Khazanov, A. Sergeev, J. C. Kieffer, G. Mourou, High energy femtosecond pulse compression, Laser Phys. Lett 13 (2016) 075401.